



## Research Paper

Effects of Ce substitution at the A-site of  $\text{LaNi}_{0.5}\text{Fe}_{0.5}\text{O}_3$  perovskite on the enhanced catalytic activity for dry reforming of methane

Meng Wang, Tingting Zhao, Xiaolei Dong, Ming Li, Haiqian Wang\*

Hefei National Laboratory for Physical Sciences at the Microscale, University of Science and Technology of China, Hefei, Anhui 230026, People's Republic of China



## ARTICLE INFO

## Keywords:

Dry reforming of methane

Ce substitution

Perovskite

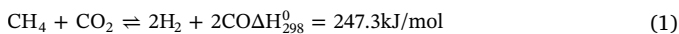
 $\text{CeO}_2$ 

## ABSTRACT

Effects of Ce substitution at the A-site of  $\text{LaNi}_{0.5}\text{Fe}_{0.5}\text{O}_3$  perovskite on the enhanced catalytic activity for dry reforming of methane (DRM) were studied.  $\text{La}_{1-x}\text{Ce}_x\text{Ni}_{0.5}\text{Fe}_{0.5}\text{O}_3$  mixed-oxide catalyst precursors were synthesized by a sol-gel self-combustion method. The  $\text{CH}_4$  and  $\text{CO}_2$  conversions increase for the samples with  $x = 0.4\text{--}0.6$ . The used catalysts consist of Ni,  $\text{CeO}_2$ , and  $(\text{LaCe})(\text{NiFe})\text{O}_3$ . The metallic Ni phase provides the primary catalytic activity, while  $(\text{LaCe})(\text{NiFe})\text{O}_3$  perovskite dominates the enhanced catalytic activity. It is confirmed that the solubility of Ce in the perovskite is high under the DRM conditions. Our results suggest that the  $\text{Ce}^{3+}$  cation at the A-site of  $(\text{LaCe})(\text{NiFe})\text{O}_3$  is active for DRM, and the relevant mechanisms are discussed.

## 1. Introduction

In recent years, dry reforming of methane (DRM) has received considerable attention. In this reaction, two greenhouse gases ( $\text{CH}_4$  and  $\text{CO}_2$ ) convert to synthesis gas with a theoretical  $\text{H}_2/\text{CO}$  ratio of 1, which is suitable for the Fischer–Tropsch synthesis [1,2]. The main reaction of DRM is [3]:



The DRM reaction (Eq (1)) needs to be carried out at high temperatures due to its endothermic nature, and thus induces the occurrence of reverse water-gas shift reaction (RWGS, Eq (2)), which leads to a higher conversion of  $\text{CO}_2$  than that of  $\text{CH}_4$  and a  $\text{H}_2/\text{CO}$  ratio lower than unity.



Noble metals are widely investigated as active metals for DRM because of the high catalytic activity [4–9], but their industrial application is limited due to the high cost. Ni-based catalyst is a good alternative to noble metals in terms of high catalytic activity, relative abundance and low cost. However, simple Ni-based catalysts tend to be deactivated due to sintering of Ni particles and severe carbon deposition during the DRM reaction [10]. Perovskites with Ni at the B-site are used as catalyst precursors to overcome these drawbacks [11–13]. Previous literature studies have shown that by using  $\text{LaNiO}_3$  as a catalyst precursor, highly dispersed small Ni particles supported on  $\text{La}_2\text{O}_3$  are formed *in situ* during the reaction, showing enhanced catalytic activity and carbon resistance in comparison with the impregnated

catalysts [14]. However,  $\text{LaNiO}_3$  decomposes completely during the DRM reaction and the Ni– $\text{La}_2\text{O}_3$  interaction is usually not strong enough to prevent Ni from sintering and carbon deposition [15–19]. Several recent studies have shown that Ni sintering and carbon deposition can be greatly suppressed by controlling the shape and structure of  $\text{LaNiO}_3$  precursors [20] or by partial substitution of the Ni-containing perovskite [21]. It is known that the B-site partial substitution of Fe in  $\text{LaNiO}_3$  can stabilize the perovskite structure, so that the  $\text{La}(\text{NiFe})\text{O}_3$  perovskite structure survives during the DRM reaction and stabilizes the long-term performance by providing stronger metal-support interaction [22–25]. Unfortunately, partial substitution of Fe in  $\text{LaNiO}_3$  decreases the catalytic activity [15,24]. Therefore, exploring Ni-based catalysts with good stability and enhanced catalytic activity still remains an open question.

Besides acting as a support, it is widely accepted that a perovskite may also show high catalytic activity on itself [26,27]. The transition metal ions at B-site are generally believed to be active for catalysis because they can interact with gas molecules (reactants and intermediates) through a set of d orbitals [28]. The role of the rare-earth cations at the A-site is considered to be less decisive as long as they are trivalent [29]. However, it is confirmed that aliovalent substitution at the A-site may remarkably enhance the catalytic activity of the perovskite through the mechanisms of modifying the electronic state of the B-site cations and/or introducing oxygen vacancies [29,30].

The valence alternation ability of  $\text{Ce}^{3+}/\text{Ce}^{4+}$  makes  $\text{CeO}_2$  a good oxygen storage material, which shows high catalytic activity for the DRM reaction [31,32]. However, the solubility of Ce in  $\text{LaMeO}_3$  (Me represents transition metals) perovskite is reported to be very low

\* Corresponding author.

E-mail address: [hqwang@ustc.edu.cn](mailto:hqwang@ustc.edu.cn) (H. Wang).

[16,33]. Nevertheless, improved catalytic activity has been reported for the perovskites with Ce-substitution of La at the A-site. For example, Sun et al. observed enhanced catalytic activity of  $(La_{0.9-x}Ce_x)FeO_3$  for water-gas shift (WGS) reaction [34]. Bliek et al. reported that the activity of  $(La_{0.8}Ce_{0.2})MnO_3$  is much higher than  $LaMnO_3$  for CO oxidation [35]. Choi et al. reported that Ce-substitution in  $La(Fe_{0.7}Ni_{0.3})O_3$  enhances the catalytic activity towards steam reforming of methane [36]. Possible explanations for the enhanced activity include [31,34–36]: (1) formation of cation/anion vacancies near the surface of the perovskite, (2) synergistic catalysis effect contributed by the redox property of  $CeO_2$ , which exists as a separate phase in the mixed-oxide, and (3) improvements of metal dispersion and the specific surface areas. It is interesting to note that La, which is believed to be catalytically inactive at the A-site of perovskites [28,37], has only one stable oxidation state ( $La^{3+}$ ). While Ce has two stable oxidation states ( $Ce^{3+}$  and  $Ce^{4+}$ ), in which f-shells are partially occupied or empty, respectively [38]. How will the switching of Ce between its two oxidation states affect the catalytic properties of the  $La_{1-x}Ce_xNi_{0.5}Fe_{0.5}O_3$  mixed-oxide? Is it possible that the A-site Ce in the perovskite is also catalytically active for the DRM reaction? Extended knowledge on these issues will be certainly helpful for exploring high performance catalysts.

In the present work,  $La_{1-x}Ce_xNi_{0.5}Fe_{0.5}O_3$  mixed-oxide catalyst precursors were synthesized by a sol-gel self-combustion method. Enhanced performance of the catalysts with  $x = 0.4$ – $0.6$  is observed. Effects of Ce substitution on the catalytic activity for the DRM reaction are discussed.

## 2. Experimental

### 2.1. Preparation of catalyst precursors (fresh catalysts)

Mixed-oxide catalyst precursors with the nominal composition of  $La_{1-x}Ce_xNi_{0.5}Fe_{0.5}O_3$  ( $x = 0.0$ – $1.0$ ) were prepared by a sol-gel self-combustion method, in which citric acid ( $C_6H_8O_7 \cdot H_2O$ ) was used as complexing agent. The starting materials were  $La_2O_3$ ,  $Ce(NO_3)_3 \cdot 6H_2O$ ,  $Ni(NO_3)_2 \cdot 6H_2O$ ,  $Fe(NO_3)_3 \cdot 9H_2O$  and  $C_6H_8O_7 \cdot H_2O$ , which were purchased from Sinopharm Chemical Agent Company. All the chemicals were of analytical grade and used directly without any further purification.  $La_2O_3$  was dissolved in distilled water by adding nitrate acid under constant stirring.  $Ce(NO_3)_3 \cdot 6H_2O$ ,  $Ni(NO_3)_2 \cdot 6H_2O$ ,  $Fe(NO_3)_3 \cdot 9H_2O$  and  $C_6H_8O_7 \cdot H_2O$  were added successively and the molar ratio between  $C_6H_8O_7 \cdot H_2O$  and the total metal ions ( $La^{3+}$ ,  $Ce^{3+}$ ,  $Ni^{2+}$  and  $Fe^{3+}$ ) was set as 1.5:1. Then the pH of the solution was adjusted to 7.0 by adding aqueous ammonia. After stirring for 12 h, the solution was heated on a heating plate until it ignited. The obtained powder in the spongy form was collected and calcined in air at 950 °C for 4 h. Thus prepared catalyst precursors were collected for further use.

### 2.2. Characterization

X-ray diffraction (XRD) analysis was performed in a 20 scan range of 20–80° by using an X-ray diffractometer (TTR III, Rigaku Co., Japan) with standard  $CuK\alpha$  radiation ( $\lambda = 1.5406 \text{ \AA}$ ). The microstructures of the samples were characterized by transmission electron microscopy (TEM, JEM-2011, JEOL, Japan).

The temperature-programmed reduction (TPR) was conducted by a simultaneous thermal analyzer (STA 449 F3, NETZSCH, Germany). During the test, samples of 10–15 mg in weight were placed in an alumina crucible and heated in 5%  $H_2/N_2$  forming gas with a flow rate of 60 ml/min. The TPR profiles were recorded from 30 to 1100 °C at a heating rate of 5 °C/min. Temperature-programmed oxidation (TPO) was performed by using the same thermal analyzer.

### 2.3. Catalytic reaction

The reaction was carried out in a fixed bed quartz reactor

(i.d. = 6 mm) at atmospheric pressure under a continuous feed of an equimolecular  $CO_2/CH_4$  mixture flowing at a rate of 60 ml/min ( $GHSV = 1.2 \times 10^4 \text{ ml/g h}$ ) without dilution. The quartz reactor was mounted vertically inside a furnace. The catalyst (300 mg) was loaded in the quartz reactor without dilution. Prior to the reaction, the precursors were reduced by pure  $H_2$  with a flow rate of 30 ml/min at 700 °C for 2 h. After purging by  $N_2$  for 30 min, the steady-state measurements were performed at 750 °C for 25 h. The reaction products were analyzed by an on-line gas chromatography (GC9790, FULI, China).

The conversions of  $CH_4$  and  $CO_2$ , the selectivity of  $H_2$ , and the carbon balance are defined as:

$$\text{Conv}_{CH_4} = \frac{F_{CH_4\text{in}} - F_{CH_4\text{out}}}{F_{CH_4\text{in}}} \times 100\%$$

$$\text{Conv}_{CO_2} = \frac{F_{CO_2\text{in}} - F_{CO_2\text{out}}}{F_{CO_2\text{in}}} \times 100\%$$

$$\text{Selec}_{H_2} = \frac{F_{H_2\text{out}}}{2 \times (F_{CH_4\text{in}} - F_{CH_4\text{out}})} \times 100\%$$

$$\text{Carbon Balance} = \frac{F_{CH_4\text{out}} + F_{CO_2\text{out}} + F_{CO\text{out}}}{F_{CH_4\text{in}} + F_{CO_2\text{in}}} \times 100\%$$

where  $F_{CH_4\text{in}}$  and  $F_{CO_2\text{in}}$  refer to the molar flow rates of the introduced  $CH_4$  and  $CO_2$ ,  $F_{CH_4\text{out}}$ ,  $F_{CO_2\text{out}}$ ,  $F_{H_2\text{out}}$  and  $F_{CO\text{out}}$  refer to the molar flow rates of  $CH_4$ ,  $CO_2$ ,  $H_2$  and  $CO$  in the tail gas.

## 3. Results

### 3.1. Catalytic performance

Fig. 1(a)–(c) show the  $CH_4$ ,  $CO_2$  conversions and  $H_2/CO$  ratio as a function of reaction time during DRM over  $La_{1-x}Ce_xNi_{0.5}Fe_{0.5}O_3$  with different  $x$  values. All the samples are active for DRM. The  $CH_4$ ,  $CO_2$  conversions and the  $H_2/CO$  ratio change slightly with reaction time at the beginning, but become quite steady after 10 h's reaction. Fig. 1(d) summarizes the values of the  $CH_4$ ,  $CO_2$  conversions,  $H_2/CO$  ratio,  $H_2$  selectivity and carbon balance (at the reaction time of 25 h), which are plotted as a function of the Ce content ( $x$ ) in the mixed-oxide. It is seen that for all the samples, the  $CO_2$  conversion is higher than the  $CH_4$  conversion, and the  $H_2/CO$  ratio is smaller than 1, suggesting the RWGS reaction is predominant in the side reactions. The changing trends of the  $CH_4$ ,  $CO_2$  conversions, the  $H_2/CO$  ratio and the  $H_2$  selectivity with  $x$  are the same. As  $x$  increases from 0.0 to 0.6, the  $CH_4$  conversion of the samples increases from 47% to 62%, the  $CO_2$  conversion increases from 59% to 72%, and the  $H_2/CO$  ratio increases from 0.80 to 0.90 with the  $H_2$  selectivity increasing from 87% to 95%. However, further increasing  $x$  to 0.8 and 1.0 will reduce the performance of the catalyst remarkably. The carbon balances of all the samples are close to 100%, indicating that the carbon deposition should be very low. Thus, we conclude that replacing a proper amount of La with Ce in the  $La_{1-x}Ce_xNi_{0.5}Fe_{0.5}O_3$  mixed-oxide has an obvious effect on enhancing the performance of the catalysts. This phenomenon agrees with other reports [35,36,39]. In order to understand the effects of Ce substitution in the  $La_{1-x}Ce_xNi_{0.5}Fe_{0.5}O_3$  mixed-oxide on the catalyst performance, we performed a series of analyses, which will be discussed in the following sections.

### 3.2. XRD analysis of the fresh and used catalysts

Fig. 2(a) shows the XRD diffraction patterns of the fresh catalysts with different  $x$  values. For the Ce-free sample ( $x = 0.0$ ), single phase  $LaNi_{0.5}Fe_{0.5}O_3$  is detected, indicating the perovskite is easily formed at 950 °C under ambient atmosphere. As  $x$  increases,  $CeO_2$ ,  $NiO$  and  $NiFe_2O_4$  appear in the mixed-oxide, and the peak intensity of the

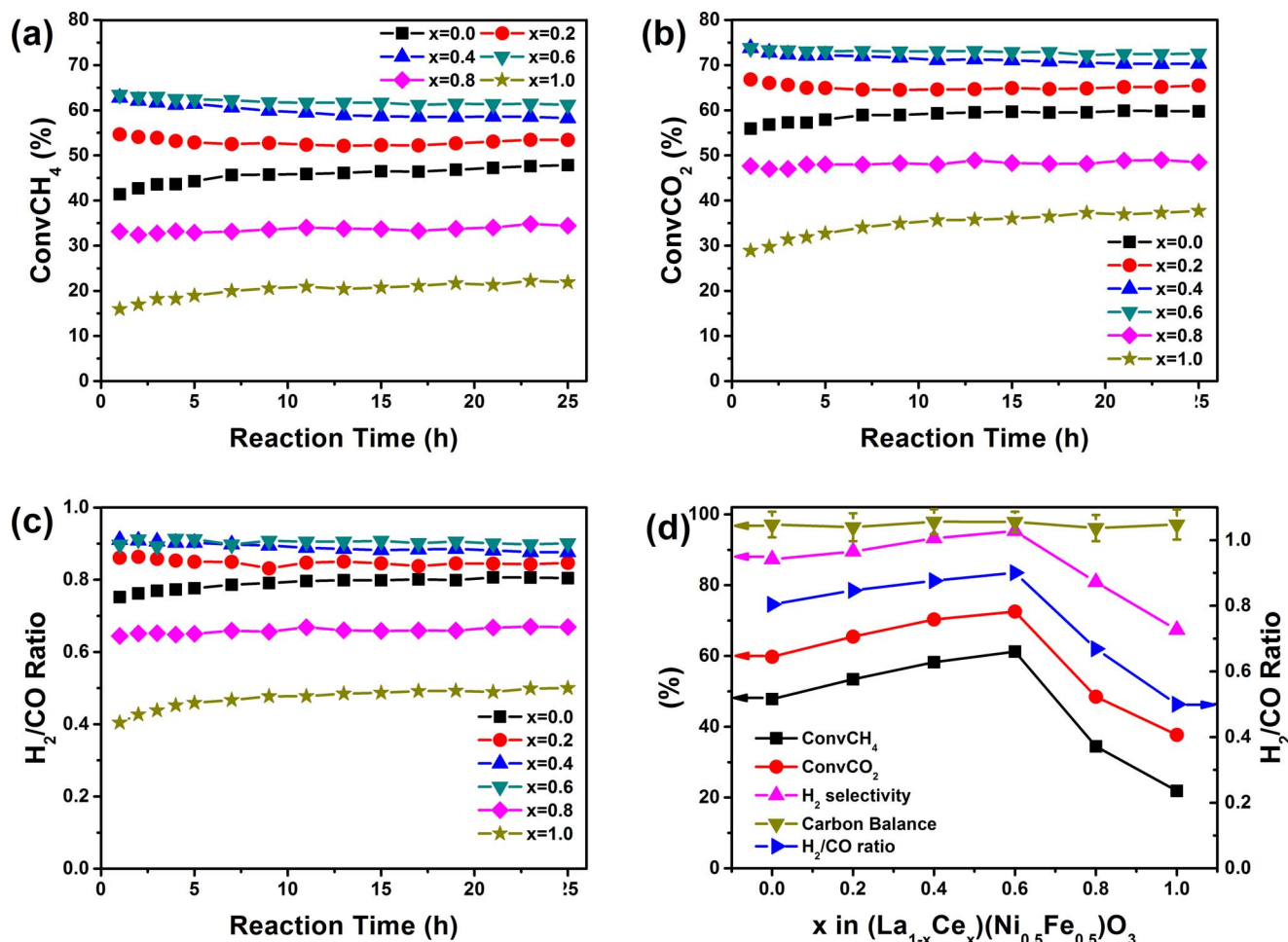


Fig. 1. (a) CH<sub>4</sub> conversion, (b) CO<sub>2</sub> conversion, and (c) H<sub>2</sub>/CO ratio as a function of reaction time during the DRM reaction over La<sub>1-x</sub>Ce<sub>x</sub>Ni<sub>0.5</sub>Fe<sub>0.5</sub>O<sub>3</sub> with different x values. (d) Changes of CH<sub>4</sub>, CO<sub>2</sub> conversions, H<sub>2</sub>/CO ratio, H<sub>2</sub> selectivity and carbon balance with x. The data reported in Fig. 1(d) are those collected at the reaction time of 25 h.

perovskite decreases. At the extreme case of x = 1.0 (La-free), only NiO, NiFe<sub>2</sub>O<sub>4</sub> spinel, and CeO<sub>2</sub> fluorite can be detected. The absence of the perovskite phase in the x = 1.0 sample indicates the solubility of Ce in the perovskite structure is very low for the fresh catalysts which were synthesized under oxidizing atmosphere.

Fig. 2(b) shows the XRD patterns of the as-reduced La<sub>1-x</sub>Ce<sub>x</sub>Ni<sub>0.5</sub>Fe<sub>0.5</sub>O<sub>3</sub> catalysts, which were reduced in pure H<sub>2</sub> at 700 °C for 2 h. For the Ce-free (x = 0.0) sample, Ni, La(NiFe)O<sub>3</sub> and La<sub>2</sub>O<sub>3</sub> are identified, indicating some of the Ni element in the perovskite can be reduced out and act as the active metallic component for DRM. For the x = 1.0 sample, diffraction peaks belonging to Ni and CeO<sub>2</sub> are clearly resolved, but no perovskite phase is detectable.

Fig. 2(c) shows the XRD diffraction patterns of the used La<sub>1-x</sub>Ce<sub>x</sub>Ni<sub>0.5</sub>Fe<sub>0.5</sub>O<sub>3</sub> catalysts. For the Ce-free (x = 0.0) sample, Ni, La(NiFe)O<sub>3</sub> and La<sub>2</sub>O<sub>2</sub>CO<sub>3</sub> are identified. It is worth noting that for the La-free (x = 1.0) sample, Ce(NiFe)O<sub>3</sub> perovskite phase is identified in addition to Ni and CeO<sub>2</sub>, even though it is absent in the corresponding fresh and as-reduced samples. It is reported that perovskites with Ce<sup>3+</sup> at the A-site can be obtained under reducing atmosphere [40,41]. Moreover, Tretyakov et al. reported that perovskites CeFeO<sub>3</sub> can only be obtained under specific range of partial oxygen pressures at high temperatures, both lower or higher partial oxygen pressures may decompose CeFeO<sub>3</sub> [42]. Under the DRM conditions (less oxidant than air but more oxidant than pure H<sub>2</sub>), some of the cerium ions exist in the form of Ce<sup>3+</sup>. The ionic radius of Ce<sup>3+</sup> (0.134 nm, 12-fold coordinated) is much larger than that of Ce<sup>4+</sup> ions (0.114 nm) and very close to the radius of La<sup>3+</sup> (0.136 nm) [43]. Thus, the observation of Ce(NiFe)O<sub>3</sub> in the used sample indicates that the DRM conditions facilitates the

incorporation of Ce into the perovskite. Considering the increased solubility of Ce<sup>3+</sup> in the perovskite under the DRM conditions, it is reasonable to deduce that the detected perovskites are in the form of (LaCe)(NiFe)O<sub>3</sub> when La and Ce coexist (x = 0.2–0.8). Thus, these catalysts are composed of a metallic phase (Ni) and an oxide phase (CeO<sub>2</sub> and (LaCe)(Ni Fe)O<sub>3</sub>).

Fig. 2(d) shows the (111) diffraction peak of Ni in the used catalysts. The (111) peak of Ni shifts progressively to lower angles with the increase of x, indicating the formation of NiFe alloy [24]. The Fe content in the NiFe alloy can be determined by analyzing the position of the XRD diffraction peak (see supplementary information Fig. S1). The Fe:Ni ratio in the alloy increases with x, but the content of Fe is much lower than that of Ni (see Table S1) in all the alloys. The lower Fe content in the alloy is because the stability of LaFeO<sub>3</sub> is much higher than that of LaNiO<sub>3</sub> under the DRM conditions [44]. It is also seen from Fig. 2(c) that once Ce is added into the mixed-oxide (x = 0.2–1.0), only Ni, CeO<sub>2</sub> and the perovskite phase are detected, while La<sub>2</sub>O<sub>2</sub>CO<sub>3</sub> is no longer detectable. A close examination on the (111) diffraction peak position of CeO<sub>2</sub> indicates that when x changes from 0.2 to 1.0, it shifts from 28.18° to the standard CeO<sub>2</sub> (111) peak position of 28.56°. This is because La<sub>2</sub>O<sub>3</sub> reacts with CeO<sub>2</sub> and forms (LaCe)O<sub>2</sub> when the content of La in the mixed-oxide is high, which has also been confirmed by Cui et al. [45].

Fig. 2(e) and (f) compare the (101) XRD diffraction peak of the perovskites in the fresh and used catalysts. As x increases, the peak of the La(NiFe)O<sub>3</sub> perovskite in the fresh catalysts shifts to lower angles and approaches that of the standard LaFeO<sub>3</sub> (see Fig. 2(e)), indicating the Fe:Ni ratio in the perovskite increases with x. For the used catalysts,

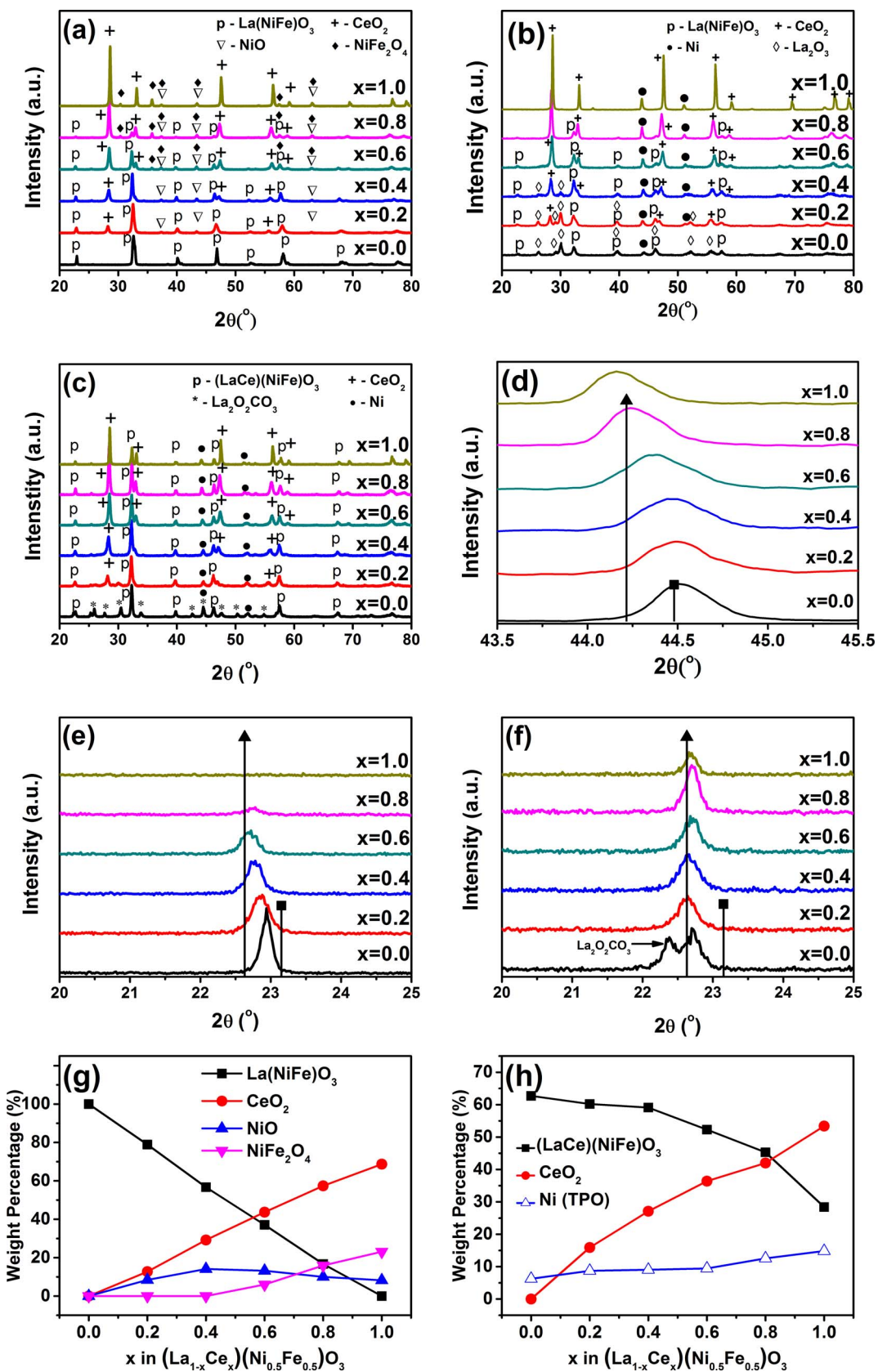


Fig. 2. XRD patterns of (a) fresh, (b) as-reduced, and (c) used  $\text{La}_{1-x}\text{Ce}_x\text{Ni}_{0.5}\text{Fe}_{0.5}\text{O}_3$  with different  $x$  values. (d) Enlarged (111) diffraction peak of the Ni phase of used catalysts with the reference phases  $\text{Ni}_3\text{Fe}$  (▲ – JCPDS 88-1715) and  $\text{Ni}$  (■ – JCPDS 70-1849). Enlarged (101) diffraction peak of the perovskite phase of (e) fresh and (f) used catalysts with the reference phases  $\text{LaFeO}_3$  (■ – JCPDS 75-0541) and  $\text{LaNiO}_3$  (▲ – JCPDS 88-0633). The composition of (g) fresh and (h) used catalysts.

the (101) diffraction peaks for all the samples are very close to that of the standard  $\text{LaFeO}_3$ , and no obvious shift can be observed (see Fig. 2(f)). However, we cannot conclude that the composition of the perovskite in the used catalysts is or close to  $\text{LaFeO}_3$ . For the used catalysts, the peak position of the perovskite may be influenced by many factors, including (1) the incorporation of  $\text{Ce}^{3+}$  into the A-site, (2) the Fe:Ni ratio in the  $(\text{LaCe})(\text{NiFe})\text{O}_3$ , (3) the enlarged ionic radius of  $\text{Ni}^{2+}$  (in the reduced form, as compared with  $\text{Ni}^{3+}$ ) and (4) the loss of the lattice oxygen. Apart from the peak position, the relative peak intensity gives us information about the stability of the perovskite phase. It is obvious that the peak intensity of the perovskite in the fresh catalysts decreases quickly with the increase of  $x$  (Fig. 2(e)). On the contrary, the peak intensity of the perovskite in the used catalysts is much more stable (Fig. 2(f)). This further confirms that the  $(\text{LaCe})(\text{NiFe})\text{O}_3$  perovskite phase stably exists under the DRM conditions.

The compositions of the fresh catalysts are quantitatively estimated by the reference intensity ratio (RIR) method [46] and the results are presented in Fig. 2(g). It is seen that in the fresh catalysts, the content of the perovskite decreases linearly with  $x$ , while that of  $\text{CeO}_2$  increases linearly with  $x$ . Fig. 2(g) also indicates that the contents of  $\text{NiO}$  and  $\text{NiFe}_2\text{O}_4$  increase with  $x$ . It is noted that  $\text{NiO}$  segregates at a smaller  $x$  value than  $\text{NiFe}_2\text{O}_4$ , indicating that the stability of Fe at the B-site of the perovskite is higher than Ni, which consists with the change of XRD peak position shown in Fig. 2(e).

Fig. 2(h) shows the compositions of the used catalysts with different  $x$  values. The contents of  $\text{CeO}_2$  and  $(\text{LaCe})(\text{NiFe})\text{O}_3$  are determined by the RIR method, while the content of Ni is determined by the TPO analysis (see supplementary information Fig. S4), which is more reliable than the RIR method. As  $x$  increases from 0.0 to 1.0, the Ni content increases from 6% to  $\sim 14\%$ , while the  $(\text{LaCe})(\text{NiFe})\text{O}_3$  content decreases from  $\sim 62\%$  to  $\sim 28\%$  and the  $\text{CeO}_2$  content increases from 0 to  $\sim 53\%$ , indicating the oxide phase changes from  $(\text{LaCe})(\text{NiFe})\text{O}_3$ -rich to  $\text{CeO}_2$ -rich as  $x$  increases.

### 3.3. Microstructures of the used catalysts

We performed TEM observations and the typical images are shown in Fig. 3. As  $x$  increases from 0.0 to 1.0, the morphologies of the samples change from aggregated “worm-like” to “pancake-like”, corresponding to the change of the oxide phase from  $(\text{LaCe})(\text{NiFe})\text{O}_3$ -rich to  $\text{CeO}_2$ -rich. No carbon deposition was observed for all the samples, which agrees with our carbon balance (see Fig. 1(d)) and TPO analyses (see supplementary information Fig. S4). Besides, Ni particles distributed on the oxide phase can be clearly resolved. The insets of Fig. 3 show the particle size distribution of Ni, which is statistically analyzed based on the TEM images over more than 150 particles. As  $x$  increases from 0.0 to 1.0, the average particle size of Ni increases from approximately 15 to 60 nm and the distribution becomes broader, indicating the metal-support interaction is getting weaker.

### 3.4. TPR

Fig. 4 shows the TPR profiles of the fresh  $\text{La}_{1-x}\text{Ce}_x\text{Ni}_{0.5}\text{Fe}_{0.5}\text{O}_3$  catalysts with different  $x$  values. As determined by the XRD analysis, the  $x = 0.0$  sample (Ce-free) is in the form of single phase perovskite  $\text{LaNi}_{0.5}\text{Fe}_{0.5}\text{O}_3$  before the TPR test. Thus, the low temperature peak (peak 1) centered at 316 °C can be attributed to the reduction of  $\text{Ni}^{3+}$  to  $\text{Ni}^{2+}$  in the perovskite. The broad high temperature peak, which spreads from  $\sim 650$  to 1050 °C, corresponds to the reduction of  $\text{Ni}^{2+}$  and  $\text{Fe}^{3+}$  in the perovskite [24]. Furthermore, the broad high temperature peak can be well fitted with two overlapped Gaussian functions, as illustrated by the dash lines in Fig. 4. It is known that Ni is more readily being reduced out from the perovskite [44]. Therefore, peak 2 centered at  $\sim 850$  °C is ascribed to the reduction of  $\text{Ni}^{2+}$  to  $\text{Ni}^0$ , and peak 3 centered at  $\sim 950$  °C is ascribed to the reduction of  $\text{Fe}^{3+}$  in the perovskite, respectively. At  $\sim 1100$  °C,  $\text{LaNi}_{0.5}\text{Fe}_{0.5}\text{O}_3$  fully decomposes

into  $\text{NiFe}$  alloy and  $\text{La}_2\text{O}_3$ .

The effect of Ce substitution is obvious. It is seen that once La is substituted by Ce, peak 4 and peak 5 come up successively with the increase of  $x$ . Based on the XRD analysis, we know that for the  $x = 0.2$  and 0.4 samples,  $\text{NiO}$  becomes pronounced in the mixed-oxide (see Fig. 2(a)). Thus, peak 4 can be assigned to the reduction of  $\text{NiO}$  in the  $x = 0.2$  and 0.4 samples. As  $x$  further increases from 0.6 to 1.0, the results in Fig. 2(g) suggest that the content of  $\text{NiFe}_2\text{O}_4$  spinel becomes high. For analysis purpose,  $\text{NiFe}_2\text{O}_4$  spinel was synthesized by the same method as the  $\text{La}_{1-x}\text{Ce}_x\text{Ni}_{0.5}\text{Fe}_{0.5}\text{O}_3$  mixed-oxide, and its TPR profile is illustrated in Fig. S2 in the supplementary information. It appears that the reduction temperature range of  $\text{NiFe}_2\text{O}_4$  overlaps with that of  $\text{NiO}$  (see supplementary information Fig. S2). Nevertheless, the TPR profile of  $\text{NiFe}_2\text{O}_4$  can be fitted by two Gaussian functions with the low and high temperature Gaussian peaks corresponding to the reduction of  $\text{Ni}^{2+}$  and  $\text{Fe}^{3+}$  in the  $\text{NiFe}_2\text{O}_4$ , respectively [47]. Thus, for the  $x = 0.6$ –1.0 samples, peak 4 is assigned to the reduction from  $\text{Ni}^{2+}$  to  $\text{Ni}^0$  of both  $\text{NiO}$  and  $\text{NiFe}_2\text{O}_4$  and peak 5 is assigned to the reduction of  $\text{Fe}^{3+}$  to  $\text{Fe}^0$  in the  $\text{NiFe}_2\text{O}_4$ . Overall, the reduction peaks 4 and 5 contribute to the catalytically active phase of metallic Ni or  $\text{NiFe}$  alloy.

It is clear that the positions of peak 1, 2 and 3 shift to lower temperatures with the increase of  $x$ , indicating the reducibility of the perovskite is increased. As  $x$  increases, the intensities of peak 1, 2 and 3 decrease remarkably, while those of peak 4 and 5 become stronger, indicating the amount of perovskite decreases while that of  $\text{NiO}$  and  $\text{NiFe}_2\text{O}_4$  increases in the mixed-oxide, which consists with the XRD analysis. It should be mentioned that we neglected the reduction of  $\text{CeO}_2$  in the above analyses, because  $\text{CeO}_2$  can only be slightly reduced under the experimental conditions and its contribution to the TPR signal is very weak as compared with the other components (see supplementary information Fig. S2).

## 4. Discussion

Our results suggest that the performance of the  $\text{La}_{1-x}\text{Ce}_x\text{Ni}_{0.5}\text{Fe}_{0.5}\text{O}_3$  mixed-oxide catalysts strongly depends on the substitution degree of Ce. A proper amount of Ce ( $x = 0.4$ –0.6) in the  $\text{La}_{1-x}\text{Ce}_x\text{Ni}_{0.5}\text{Fe}_{0.5}\text{O}_3$  increases obviously the  $\text{CH}_4$  and  $\text{CO}_2$  conversions, as well as the  $\text{H}_2/\text{CO}$  ratio. It is believed multiple factors should be responsible for the enhanced catalytic activity of the  $x = 0.4$ –0.6 mixed-oxide catalysts.

### 4.1. The role of the metallic phase

Undoubtedly, the metallic phase in the catalysts provides the primary catalytic activity for the DRM reaction. However, the enhanced catalytic activity of the  $x = 0.4$ –0.6 catalysts should not be (or at least not completely) originated from the metallic phase. Although the mass loading of the metallic phase (Ni or  $\text{NiFe}$  alloy) in the used catalysts increases from  $\sim 6$  wt% to  $\sim 14$  wt% as  $x$  increases from 0.0 to 1.0 (Fig. 2(h)), our TEM analysis (Fig. 3) indicates that the average particle size of the metal increases from  $\sim 15$  to 60 nm simultaneously. The monotonous increase in the metallic particle size indicates the metal-support interaction is getting weaker all the way. Thus, the change in the metallic particle size/distribution due to the metal-support interaction can not explain the enhanced catalytic activity [24]. Moreover, it can be estimated that the partial specific areas of the metallic phase show an overall decreasing trend with  $x$  (see supplementary information Fig. S3). Thus, there is no evidence that the metallic phase in the  $x = 0.4$ –0.6 catalysts can provide more active reaction sites as compared with the rests.

It should also be noted that the Fe content in the  $\text{NiFe}$  alloy increases with  $x$  (see Fig. 2(d), Fig. S1 and Table S1). Kim et al. reported that the activity of  $\text{Ni}_4\text{Fe}_1$  alloy is higher than monometallic Ni due to the enhanced carbon-resistance for the DRM reaction, and further increase in the Fe content reduces the catalytic activity [48]. Since the carbon deposition is negligible in the present experiments (see Fig. 1(d)),

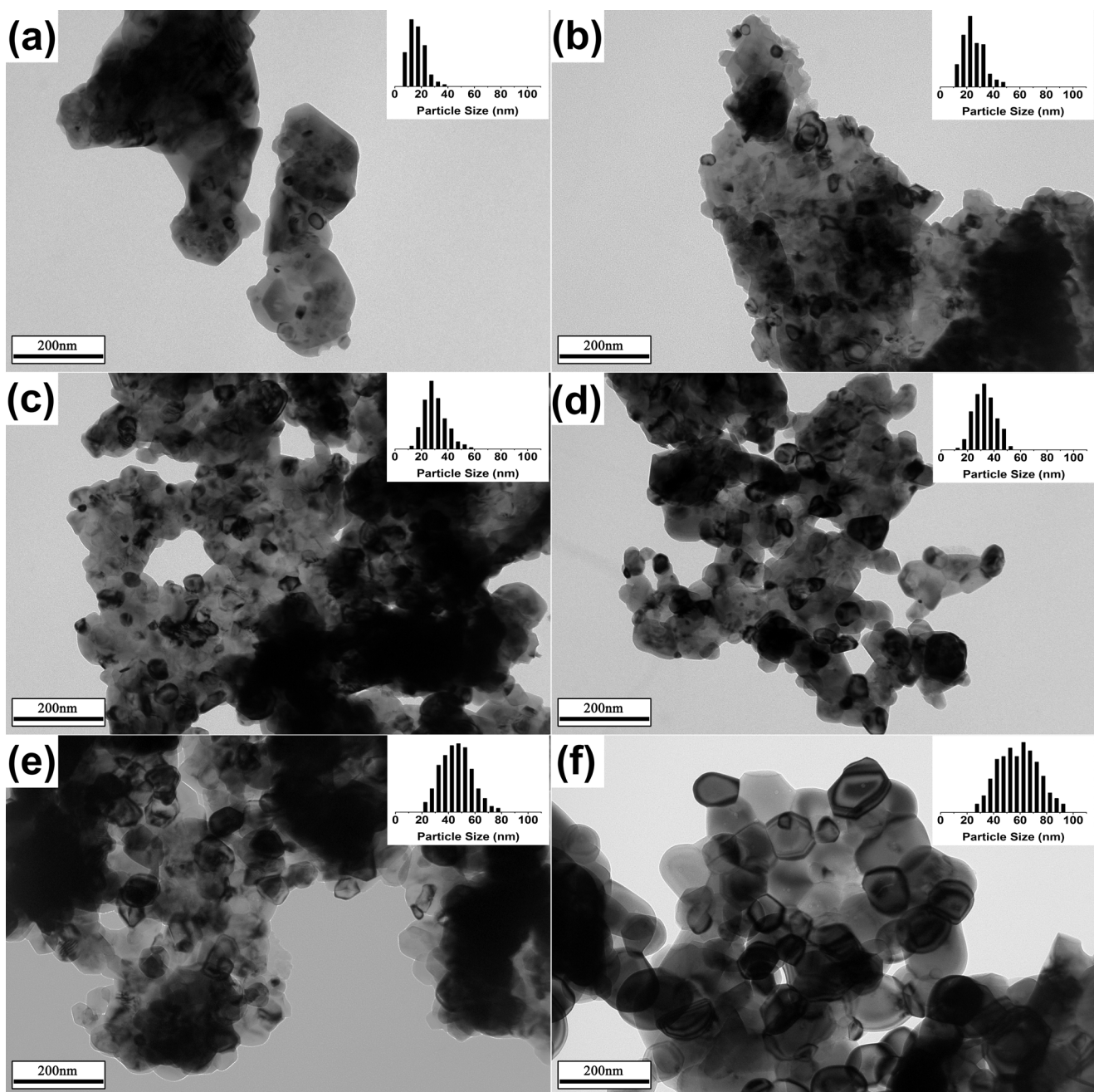


Fig. 3. Typical TEM images of used  $\text{La}_{1-x}\text{Ce}_x\text{Ni}_{0.5}\text{Fe}_{0.5}\text{O}_3$  with  $x = (a) 0.0, (b) 0.2, (c) 0.4, (d) 0.6, (e) 0.8, \text{ and } (f) 1.0$ , respectively. The insets are the particle size distribution of Ni, which is statistically analyzed over more than 150 particles.

Fig. 3 and Fig. S4), the incorporation of Fe in the NiFe alloy will not enhance the activity by promoting the decomposition of graphitic carbon via a redox mechanism. Therefore, we can hardly attribute the enhanced performance of the catalysts at about  $x = 0.4\text{--}0.6$  to the metallic phase.

#### 4.2. The role of $\text{CeO}_2$

High catalytic activity of  $\text{CeO}_2$  for the DRM reaction is reported [31,32]. It is closely related to its oxygen storage capacity, namely, the ability of undergoing rapid and repeatable redox cycles. There is an agreement that  $\text{CeO}_2$  catalyzes the DRM reaction through a redox mechanism:  $\text{CeO}_2$  decomposes  $\text{CH}_4$  into  $\text{CO}$  and  $\text{H}_2$ , and itself is reduced into  $\text{CeO}_{2-\delta}$ ;  $\text{CeO}_{2-\delta}$  reacts with  $\text{CO}_2$  to produce  $\text{CO}$ , and the reduced  $\text{CeO}_{2-\delta}$  is oxidized into  $\text{CeO}_2$  again [31,32,49,50]. However, the content

of  $\text{CeO}_2$  increases monotonously with  $x$ , and the samples with larger  $\text{CeO}_2$  content ( $x = 0.8$  and  $1.0$ ) show a declined activity. Besides, it is also known that  $\text{CeO}_2$  is prone to sintering and will result in a degradation in the catalytic performance during the DRM reaction [32]. We didn't observe obvious degradation in both the  $\text{CH}_4$  and  $\text{CO}_2$  conversions (see Fig. 1) in the present work, implying the activity of  $\text{CeO}_2$  may not be the reason for the enhanced catalytic activity of the mixed-oxide.

#### 4.3. The role of $(\text{LaCe})(\text{NiFe})\text{O}_3$

In the present work, the perovskite exists in the form of  $(\text{LaCe})(\text{NiFe})\text{O}_3$  during the DRM reaction. When  $x = 0.4\text{--}0.6$ , the amount of  $(\text{LaCe})(\text{NiFe})\text{O}_3$  is greater than 50% (Fig. 2(h)). It is reported that enhanced catalytic activity of a perovskite is related to its increased

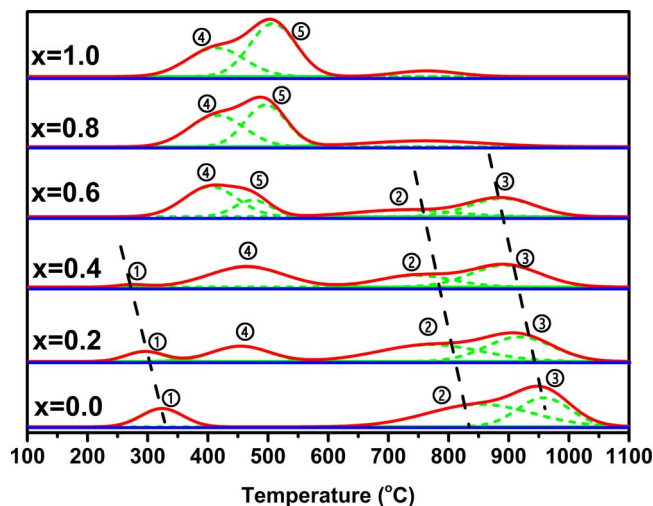


Fig. 4. TPR profiles of fresh  $\text{La}_{1-x}\text{Ce}_x\text{Ni}_{0.5}\text{Fe}_{0.5}\text{O}_3$  with different  $x$  values.

reducibility [11,12,51,52]. According to our TPR analysis (Fig. 4), as  $x$  increases, the positions of peak 1, 2 and 3 all shift to lower temperatures, suggesting that the catalytic activity of the perovskite should become higher. The predominant content of the perovskite, together with the increased activity, suggests that the perovskite should play an important role in the enhanced catalytic activity of the  $x = 0.4\text{--}0.6$  catalysts.

Synergic catalytic effects between the active metallic phase and the oxide phase (support) are widely accepted for DRM:  $\text{CH}_4$  is activated on the metal and  $\text{CO}_2$  is activated on the support. It is also believed that the activation of  $\text{CO}_2$  depends on the surface Lewis acidity-basicity of the oxide support. On acidic supports,  $\text{CO}_2$  is activated through the formation of formates by the reaction between  $\text{CO}_2$  and the surface hydroxyls [53]; while on basic supports,  $\text{CO}_2$  is activated by forming carbonates [54]. It is reported that the activation of the mildly acidic  $\text{CO}_2$  on basic supports is stronger than on acidic supports [8]. As evidenced by the TPR analysis (Fig. 4),  $\text{Ni}^{3+}$  in  $(\text{LaCe})(\text{NiFe})\text{O}_3$  tends to be reduced into  $\text{Ni}^{2+}$ . Consequently, oxygen loss must occur to compensate the electric neutrality. Thus, large amount of oxygen vacancies must be introduced into the  $(\text{LaCe})(\text{NiFe})\text{O}_3$  both in the bulk and on the surface. These oxygen vacancies are Lewis basic [55] and the oxygen vacancies on the surface can act as active sites for  $\text{CO}_2$  activation.

Another possible mechanism for the enhanced catalytic activity is that the  $(\text{LaCe})(\text{NiFe})\text{O}_3$  perovskite is active for the DRM reaction alone. High catalytic activity of perovskites has been proven by many researches [26,27]. It is reported that  $\text{CH}_4$  oxidation over a perovskite follows the Mars-van Krevelen mechanism involving consumption of lattice oxygen and its backfilling from the gas phase oxidant [56]. In most cases, oxygen vacancies are the dominant defects in a perovskite, especially under the relatively reducing environment of DRM. These oxygen vacancies act as the active sites for dissociative adsorption and activation of the reactants and intermediates [11,57,58]. In the case of DRM,  $\text{CO}_2$  adsorbs dissociatively into  $\text{CO}$  and  $\text{O}$ , and  $\text{O}$  replenishes the oxygen vacancies [59]. In addition, oxygen vacancies in  $(\text{LaCe})(\text{NiFe})\text{O}_3$  also increase the oxygen mobility in the lattice, thus promote the backfilling of lattice oxygen through the Mars-van Krevelen mechanism and increase the catalytic activity of the perovskite.

Usually, the catalytic activity of a perovskite is largely determined by the B-site cation [29]. Under the DRM conditions, undercoordinated metal cations, together with oxygen vacancies, are formed by the removal of the lattice oxygen. The undercoordinated metal cations are metallic like and act as additional active sites for  $\text{CH}_4$  adsorption and dissociation [60]. In  $(\text{LaCe})(\text{NiFe})\text{O}_3$ , the Fe cation should be mainly responsible for the stabilization of the perovskite lattice structure, while Ni cation should be largely responsible for the activity.

Apart from the transition metal cations at the B-site, it is more interesting to note that the DRM-active  $\text{Ce}^{3+}$  cation exists at the A-site of  $(\text{LaCe})(\text{NiFe})\text{O}_3$  [31]. Since  $\text{Ce}^{3+}$  has the same valence state as  $\text{La}^{3+}$ , it cannot introduce more oxygen vacancies directly into the perovskite in the way a lower-valence cation does [11]. However, as evidenced by our TPR analysis (Fig. 4), peak 1 and 3 (which belong to the reduction of  $\text{Ni}^{3+}$  and  $\text{Fe}^{3+}$ ) both shift to lower temperatures as  $x$  increases, indicating the transition metal cations at the B-site are more reducible due to the incorporation of  $\text{Ce}^{3+}$  at the A-site. Thus, we can say that the  $\text{Ce}^{3+}$  cation at the A-site indirectly introduce more oxygen vacancies into  $(\text{LaCe})(\text{NiFe})\text{O}_3$  by activating the B-site cations, which is beneficial for the enhancement of the catalytic activity.

Ce is known to have two stable oxidation states, namely,  $\text{Ce}^{4+}$  and  $\text{Ce}^{3+}$ , in which the f-shells are empty or partially occupied, respectively. Theoretical studies on reduced ceria suggest that once a neutral oxygen vacancy is created, the two electrons left behind reduce the two nearest neighboring Ce atoms of the oxygen vacancy. The change of f-electrons from valence ( $\text{Ce}^{4+}$ ) to core-like ( $\text{Ce}^{3+}$ ) leads to localized electrons in atomic-like orbitals [38]. The same idea should also be applicable to  $(\text{LaCe})(\text{NiFe})\text{O}_3$ , in which Ce particularly tends to exist in the form of  $\text{Ce}^{3+}$ . Thus it is possible that the atomic-like orbitals of  $\text{Ce}^{3+}$  at the A-site are stabilized by the  $(\text{LaCe})(\text{NiFe})\text{O}_3$  perovskite structure and enhance the catalytic activity.

Moreover, the large difference in the solubility of  $\text{Ce}^{3+}$  in the perovskite between the oxidizing and relatively reducing environments (Fig. 2) facilitates the redox cycles of  $\text{Ce}^{3+}/\text{Ce}^{4+}$ , which is also beneficial for the DRM reaction over  $(\text{LaCe})(\text{NiFe})\text{O}_3$  through a redox mechanism. As evidenced by our XRD analysis,  $(\text{LaCe})(\text{NiFe})\text{O}_3$  and  $\text{CeO}_2$  exist as two separate phases, which are stable under relatively reducing and oxidizing environments, respectively. For the mixed-oxide material system present in this work,  $(\text{LaCe})(\text{NiFe})\text{O}_3$  acts as the reservoir of  $\text{Ce}^{3+}$ , while  $\text{CeO}_2$  acts as the reservoir of  $\text{Ce}^{4+}$ . Thus, Ce cations ( $\text{Ce}^{3+}/\text{Ce}^{4+}$ ) will reversibly shuttle between  $(\text{LaCe})(\text{NiFe})\text{O}_3$  and  $\text{CeO}_2$  depending on the local redox fluctuations. This is somewhat like the self-regeneration effect of a perovskite, which refers to the migration of the B-site transition metal inside-outside of the perovskite and refreshes the transition metal particles at the perovskite surface [25,61]. Although we didn't observe any self-regeneration effect on the B-site transition metal of  $(\text{LaCe})(\text{NiFe})\text{O}_3$ , it's very likely that the so-called "self-regeneration" occurs at the A-site in a different way.

## 5. Conclusions

$\text{La}_{1-x}\text{Ce}_x\text{Ni}_{0.5}\text{Fe}_{0.5}\text{O}_3$  mixed-oxide catalyst precursors were synthesized by a sol-gel self-combustion method, and obviously enhanced catalytic activity for the DRM reaction was observed by replacing a proper amount of La with Ce in the mixed-oxide. The used catalysts consist of Ni,  $\text{CeO}_2$ , and  $(\text{LaCe})(\text{NiFe})\text{O}_3$ . Our results suggest that the metallic Ni phase provides the primary catalytic activity, while the  $(\text{LaCe})(\text{NiFe})\text{O}_3$  perovskite dominates the enhanced catalytic activity. We propose that the  $\text{Ce}^{3+}$  cation at the A-site of  $(\text{LaCe})(\text{NiFe})\text{O}_3$  improves the catalytic activity of the perovskite (1) by introducing more oxygen vacancies by activating the B-site cations, and/or (2) through a redox mechanism, in which  $\text{Ce}^{3+}/\text{Ce}^{4+}$  cations reversibly shuttle between  $(\text{LaCe})(\text{NiFe})\text{O}_3$  and  $\text{CeO}_2$  depending on the local redox fluctuations. The large difference in the solubility of Ce in the perovskite between the oxidizing and relatively reducing environments provides the essential driving force for the exchange of the Ce element between  $\text{CeO}_2$  and the perovskite.

## Acknowledgement

This work is supported by the National Natural Science Foundation of China (Grant No.: 21427804)

## Appendix A. Supplementary data

Supplementary data associated with this article can be found, in the online version, at <http://dx.doi.org/10.1016/j.apcatb.2017.10.022>.

## References

- [1] D.L. Trimm, Catal. Rev. Sci. Eng. 16 (1977) 155–189.
- [2] I. Wender, Fuel Process. Technol. 48 (1996) 189–297.
- [3] Y. Vafaeian, M. Haghghi, S. Aghamohammadi, Energy Convers. Manag. 76 (2013) 1093–1103.
- [4] M.C.J. Bradford, M.A. Vannice, J. Catal. 173 (1998) 157–171.
- [5] M.C.J. Bradford, M.A. Vannice, J. Catal. 183 (1999) 69–75.
- [6] A. Erdohelyi, J. Cserenyi, E. Papp, F. Solymosi, Appl. Catal. a-General. 108 (1994) 205–219.
- [7] M.F. Mark, W.F. Maier, J. Catal. 164 (1996) 122–130.
- [8] D. Pakhare, J. Spivey, Chem. Soc. Rev. 43 (2014) 7813–7837.
- [9] V.A. Tsipouriaris, A.M. Efstathiou, Z.L. Zhang, X.E. Verykios, Catal. Today 21 (1994) 579–587.
- [10] J.R. RostrupNielsen, J.H.B. Hansen, J. Catal. 144 (1993) 38–49.
- [11] J.J. Zhu, H.L. Li, L.Y. Zhong, P. Xiao, X.L. Xu, X.G. Yang, Z. Zhao, J.L. Li, ACS Catal. 4 (2014) 2917–2940.
- [12] S. Royer, D. Duprez, F. Can, X. Courtois, C. Batiot-Dupeyrat, S. Laassiri, H. Almadari, Chem. Rev. 114 (2014) 10292–10368.
- [13] E.A. Lombardo, M.A. Ulla, Res. Chem. Intermed. 24 (1998) 581–592.
- [14] G.S. Gallego, F. Mondragón, J. Barrault, J.-M. Tatibouét, C. Batiot-Dupeyrat, Appl. Catal. A Gen. 311 (2006) 164–171.
- [15] S.M. de Lima, J.M. Assaf, Catal. Lett. 108 (2006) 63–70.
- [16] S.M. Lima, J.M. Assaf, M.A. Pena, J.L.G. Fierro, Appl. Catal. A Gen. 311 (2006) 94–104.
- [17] G.S. Gallego, J.G. Marin, C. Batiot-Dupeyrat, J. Barrault, F. Mondragon, Appl. Catal. a-General. 369 (2009) 97–103.
- [18] A. Slagtern, U. Olsbye, Appl. Catal. A, Gen. 110 (1994) 99–108.
- [19] H. Provendier, C. Petit, C. Estournes, A. Kiennemann, Nat. Gas Convers. V 119 (1998) 741–746.
- [20] S. Singh, D. Zubenko, B.A. Rosen, ACS Catal. 6 (2016) 4199–4205.
- [21] D. Neagu, T.-S. Oh, D.N. Miller, H. Ménard, S.M. Bukhari, S.R. Gamble, R.J. Gorte, J.M. Vohs, J.T.S. Irvine, Nat. Commun. 6 (2015) 8120.
- [22] H. Provendier, C. Petit, C. Estournes, S. Libs, A. Kiennemann, Appl. Catal. a-General. 180 (1999) 163–173.
- [23] H. Provendier, C. Petit, A. Kiennemann, Comptes Rendus l'Academie Des Sci. IIC-Chem. 4 (2001) 57–66.
- [24] X. Song, X. Dong, S. Yin, M. Wang, M. Li, H. Wang, Appl. Catal. A Gen. 526 (2016) 132–138.
- [25] J. Deng, M.D. Cai, W.J. Sun, X.M. Liao, W. Chu, X.S. Zhao, ChemSusChem 6 (2013) 2061–2065.
- [26] T. Seiyama, Catal. Rev. 34 (1992) 281–300.
- [27] R.J.H. Voorhoeve, D.W. Johnson, J.P. Remeika, P.K. Gallagher, Science 195 (1977) 827–833.
- [28] J.L.G. Fierro, Catal. Today 8 (1990) 153–174.
- [29] M.M.T. Nitadori, T. Ichiki, Bull. Chem. Soc. Jpn. 61 (1988) 621–626.
- [30] S. Keav, S. Matam, D. Ferri, A. Weidenkaff, Catalysts 4 (2014) 226–255.
- [31] K. Otsuka, Y. Wang, E. Sunada, I. Yamanaka, J. Catal. 175 (1998) 152–160.
- [32] N. Laosiripojana, S. Assabumrungrat, Appl. Catal. B-Environ. 60 (2005) 107–116.
- [33] P. Erri, P. Dinka, A. Varma, Chem. Eng. Sci. 61 (2006) 5328–5333.
- [34] Y. Sun, S.S. Hla, G.J. Duffy, A.J. Cousins, D. French, L.D. Morpeth, J.H. Edwards, D.G. Roberts, Int. J. Hydrogen Energy 36 (2011) 79–86.
- [35] Y. Zhang-Steenwinkel, J. Beckers, A. Bliek, Appl. Catal. A Gen. 235 (2002) 79–92.
- [36] S.O. Choi, S.H. Moon, Catal. Today 146 (2009) 148–153.
- [37] D. Ferri, L. Forni, Appl. Catal. B Environ. 16 (1998) 119–126.
- [38] A. Hofmann, J. Sauer, Surf. Sci. Rep. 62 (2007) 219–270.
- [39] X.-P. Xiang, L.-H. Zhao, B.-T. Teng, J.-J. Lang, X. Hu, T. Li, Y.-A. Fang, M.-F. Luo, J.-J. Lin, Appl. Surf. Sci. 276 (2013) 328–332.
- [40] K. Ito, K. Tezuka, Y. Hinatsu, J. Solid State Chem. 157 (2001) 173–179.
- [41] L. Zhao, S.R. Bishop, J. Hyodo, T. Ishihara, K. Sasaki, ECS Trans. 50 (2013) 53–58.
- [42] Y.D. Tretyakov, V.V. Sorokin, A.R. Kaul, A.P. Erastova, J. Solid State Chem. 18 (1976) 253–261.
- [43] W.M. Haynes, CRC Handbook of Chemistry and Physics, CRC press, 2014.
- [44] T. Nakamura, G. Petzow, L.J. Gauckler, Mater. Res. Bull. 14 (1979) 649–659.
- [45] Y. Cui, V. Galvita, L. Rihko-Struckmann, H. Lorenz, K. Sundmacher, Appl. Catal. B Environ. 90 (2009) 29–37.
- [46] R.L. Snyder, Powder Diffrr. 7 (2013) 186–193.
- [47] R. Benrabaa, A. Löfberg, A. Rubbens, E. Bordes-Richard, R.N. Vannier, A. Barama, Catal. Today 203 (2013) 188–195.
- [48] S.M. Kim, P.M. Abdala, T. Margossian, D. Hosseini, L. Foppa, A. Armutlulu, W. van Beek, A. Comas-Vives, C. Coperet, C. Muller, J. Am. Chem. Soc. 139 (2017) 1937–1949.
- [49] A. Löfberg, J. Guerrero-Caballero, T. Kane, A. Rubbens, L. Jalowiecki-Duhamel, Appl. Catal. B Environ. 212 (2017) 159–174.
- [50] M. Tang, L. Xu, M. Fan, Appl. Energy 151 (2015) 143–156.
- [51] R. Zhang, H. Almadari, S. Kaliaguine, J. Catal. 242 (2006) 241–253.
- [52] H. Falcón, M.J. Martínez-Lope, J.A. Alonso, J.L.G. Fierro, Solid State Ionics 131 (2000) 237–248.
- [53] P. Ferreira-Aparicio, I. Rodríguez-Ramos, J.A. Anderson, A. Guerrero-Ruiz, Appl. Catal. A Gen. 202 (2000) 183–196.
- [54] R. Bouarab, O. Akdim, A. Auroux, O. Cherifi, C. Mirodatos, Appl. Catal. A Gen. 264 (2004) 161–168.
- [55] E.W. McFarland, H. Metiu, Chem. Rev. 113 (2013) 4391–4427.
- [56] A. Eyssler, A. Winkler, O. Safonova, M. Nachtegaal, S.K. Matam, P. Hug, A. Weidenkaff, D. Ferri, Chem. Mater. 24 (2012) 1864–1875.
- [57] J.A. Gómez-Cuaspud, C.A. Perez, M. Schmal, Catal. Lett. 146 (2016) 2504–2515.
- [58] J.A. Gómez-Cuaspud, E. Vera-López, J.B. Carda-Castelló, E. Barrachina-Albert, React. Kinet. Mech. Catal. 120 (2016) 167–179.
- [59] K. Urasaki, Y. Sekine, S. Kawabe, E. Kikuchi, M. Matsukata, Appl. Catal. A Gen. 286 (2005) 23–29.
- [60] Y. Zheng, K. Li, H. Wang, D. Tian, Y. Wang, X. Zhu, Y. Wei, M. Zheng, Y. Luo, Appl. Catal. B Environ. 202 (2017) 51–63.
- [61] Y. Nishihata, J. Mizuki, T. Akao, H. Tanaka, M. Uenishi, M. Kimura, T. Okamoto, N. Hamada, Nature 418 (2002) 164–167.